Vacuum 153 (2018) 225–231

Contents lists available at ScienceDirect

Vacuum

journal homepage: www.elsevier.com/locate/vacuum

Indium free electrode, highly flexible, transparent and conductive for optoelectronic devices

H. Essaidi[a,e], L. Cattin[b], Z. El Jouad[b,f], S. Touihri[a,e], M. Blais[b], E. Ortega[c], G. Louarn[b], M. Morsli[d], T. Abachi[a,g], T. Manoubi[e], M. Addou[f], M.A. del Valle[c], F. Diaz[c], J.C. Bernède[a,*]

[a] MOLTECH-Anjou, CNRS, UMR 6200, Université de Nantes, 2 rue de la Houssinière, BP 92208, Nantes, F-44322, France
[b] Institut des Matériaux Jean Rouxel (IMN), Université de Nantes, CNRS, 2 rue de la Houssinière, BP 32229, 44322, Nantes, cedex 3, France
[c] Pontificia Universidad Católica de Chile, Av.V. Mackenna 4860-Macul, BP 7820436, Santiago, Chile
[d] Faculté des Sciences et des Techniques, 2 rue de la Houssinière, BP 32229, 44322, Nantes, cedex 3, France
[e] Unité de Physique des Dispositifs à Semi-conducteurs, Université El Manar, Faculté des Sciences de Tunis, Campus Universitaire 2092, Tunis, Tunisia
[f] LMVR, FST, Université Abdelmalek Essaidi, Tanger, Ancienne Route de l'Aéroport, Km 10, Ziaten. BP: 416, Morocco
[g] ENS Kouba, B.P. 92, Vieux-Kouba, 16308, Alger, Algeria

ARTICLE INFO

Keywords:
ITO free electrode
Organic photovoltaic cells
Transparent heat mirrors
Transparent heaters
Transparent conductive electrode

ABSTRACT

WO_3/Ag/WO_3 multilayer structures were used as ITO free transparent electrode, transparent heat mirrors and transparent heaters. WO_3/Ag/WO_3 stacked layers were deposited by sequential sublimation, evaporation under vacuum. After optimization of Ag thickness (16 nm), they exhibit low sheet resistance (8 Ω/sq), high transmittance in the visible (T_{Max} = 91.5%, averaged $T_{400\text{-}700}$ = 80.6%) and high reflection in the near infrared and infrared regions. These values are optimal when it is used as transparent electrode but, as transparent heat mirrors 18 nm are better due to higher reflection in the NIR and IR. All these properties made possible to use them in different devices. When used as transparent anode in organic photovoltaic cells, they allow achieving performance similar to those obtained with ITO. Their transmission and reflection spectra show that they can also be employed as transparent heat mirrors. Similarly, studies dedicated to heating properties of the WO_3/Ag/WO_3 multilayer structures show that their performance are comparable to those obtained with another possible substituent to ITO, silver nanowires thin films.

1. Introduction

Transparent conductive electrodes (TCE) are commonly used in many optoelectronic devices such as organic photovoltaic cells (OPVCs), flat panel displays, organic light-emitting diodes (OLEDs) and sensors [1–4]. In this regard, indium Tin Oxide (ITO) films are the most often used as TCE in optoelectronic devices, due to their high transparency and good conductivity [5–7]. But the transparent conductive electrode (TCE) industry will achieve rapid growth, serving a size of more than 60 million square meter per year and indium is scarce, moreover there is currently a considerable interest in flexible electronic and ITO is brittle. Therefore it is necessary to look for Indium free TCE. New market opportunities are emerging, changing the prospects of various technologies and increasing the demand overall in the coming years. Indeed, the TCE field is entering a new phase. Some ITO alternatives have matured, such as other transparent conductive oxides, doped ZnO [8] or SnO2 [9] but also, Dielectric/Metal/Dielectric (D/M/D) multilayer structures have shown promising perspectives due to their high conductivity. For instance, ZnO/Ag/ZnO was shown to present good performance [10]. Finally, the conductivity of these structures being mainly controlled by the conductivity of the metal layer, D/M/D multilayers, using oxides others than TCO, have gained much attention as promising substituent to ITO because these structures can suppress the reflection from the metal layer, due to high refractive indexes of dielectrics, and obtain a selective transparent electrode with high conductivity. Usually, this structure consists in a thin Ag layer (10–20 nm) sandwiched between two dielectric layers [11–13]. Numerous methods of producing the new TCE are investigated. Using transition metal oxides such as MoO_3 or WO_3 allows using a simple sublimation/evaporation deposition technique for the whole multilayer structure. Due to the well known high efficiency of MoO_3 as anode buffer layer, it was often used as dielectric in such D/M/D multilayer structures, because this made it possible to directly use these structures as anodes in devices, without the need to add a buffer layer between the electrode and the organic layer. However, it was shown recently that if WO_3 is used instead of MoO_3 in optoelectronic devices, more

* Corresponding author.
E-mail address: jean-christian.bernede@univ-nantes.fr (J.C. Bernède).

https://doi.org/10.1016/j.vacuum.2018.04.026
Received 19 January 2018; Received in revised form 12 April 2018; Accepted 13 April 2018
Available online 16 April 2018
0042-207X/

reproducible and stable devices are obtained [14–16]. Therefore, in the present work, WO_3/Ag/WO_3 (W/A/W) multilayer structures were prepared and studied, before using them in different devices. If many manuscripts are dedicated to MoO_3/Ag/MoO_3 multilayer structures [12,17–19], it is possible to find some others which are devoted to W/A/W multilayer structures [20–23]. For instance, the effect of thermal annealing on the performance of W/A/W transparent conductive structures has been studied [21]. It is shown that, even for an annealing at 200 °C, the optical and electrical properties of the structures are nearly preserved, which testifies of their stability. The electrochomic properties of WO_3 being well known, W/A/W multilayer structures have also been probed successfully in ITO free electrochomic devices [22–24]. About flexibility, two main technical issues must be taken into account, flexible substrates such as PET, cannot undergo thermal processes higher than 150 °C, flexible devices must be able to suffer thousands of bending cycles without worsening their electro-optical properties. In the present work, after optimizing the optical, electrical and morphological properties of the structures, we show that it is possible to use them in several types of devices. More precisely, we show that using the Ag thickness as parameter it is possible to grow highly performing devices such as OPVCs, Transparent Heat Mirrors (THM) and Transparent Heaters (THs). In the case of OPVCs, it is necessary to use a highly conductive electrode with an optimized top layer for efficient carrier collection. On the other hand, in the case of transparent heater (TH), the electrical energy must be rapidly and efficiently converted into thermal energy. Due to its slow thermal response, ITO is not ideal. W/A/W transparent conductive structures, due to the high conductivity and thermal performance of Ag, appear far more promising. Here the problem of stability of the Ag conductor is over passed thanks to the layers of oxides that enclose the silver layer.

2. Experimental details

2.1. W/A/W multilayer structures realization and characterization

W/A/W multilayer structures were grown on both glass and 150 μm thick PET substrates using simple sublimation/evaporation technique. Before deposition, the PET substrates were underwent to a specific surface treatment in order to obtain conductive and adherent multilayer structures. After cleaning by a detergent, Micro Son (Ref 4890D) provided by Fisher Scientific, the PET substrates were rinsed in running distilled water. Then they were treated in 0.5 M NaOH at 90 °C for half an hour, rinsed again with distilled water and finally dried in an oven and introduced into the deposition apparatus. Such a treatment allows improving the adherence of functional layers on PET substrates as shown by Amendola et al. [25]. The deposition process was started for a vacuum of 10^{-4} Pa. The multilayer structures were successively deposited onto substrates at room temperature, using two tungsten crucibles, one loaded with WO_3 powder and the other one with Ag wires. The bottom WO_3 layer thickness was 20 nm following earlier studies of D/M/D structures [26], while the top WO_3 layer was between 15 and 35 nm. The thickness of this top oxide layer depends on its use, thus it will be 15 nm, since optimum results were obtained using this thickness when it serves as an anode in an OPVC and 35 nm when used in other devices. After deposition of the bottom WO_3 layer, at a deposition rate of 0.03 nm/s, Ag film was deposited by thermal evaporation at a deposition rate of 0.3 nm/s, since we have shown that this value allows obtaining optimized structures [27]. Subsequently, the top WO_3 layer was deposited at identical conditions to those used for the bottom WO_3 layer. Both film thickness and deposition rate were monitored with a quartz crystal microbalance.

Sheet resistance, R_s, of the W/A/W structures was measured at room temperature, using a four-point technique, as a function of Ag thickness. In order to obtain reproducible results we used a specific mask, which allows depositing very small area point contacts.

The optical measurements were carried out at room temperature using a UV/visible spectrometer (Perkin spectrophotometer). The optical transmission could be measured in 300 nm–2500 nm spectral range.

The thin film structures were monitored by X-ray diffraction (XRD) using a Siemens D5000 diffractometer with a Kα radiation (λ = 1,54056 °A). XRD diagrams were collected in the Bragg-Brantano orientation with a step size of 0.020 and while counting for 2 s per step.

The surface and the cross section of the W/A/W multilayer structures were observed with a field emission scanning electron microscope (SEM, JEOL F-7600). The SEM operating voltage was 5 kV. In order to improve the visualization of the cross section, images in secondary (SEM) and backscattering (BEI) modes were done ("Centre de microcaractéristion, Institut des Matériaux Jean Rouxel, Université de Nantes").

AFM images of the films were taken ex-situ at atmospheric pressure and room temperature. For each sample, the surface image was carried out in various places with a maximum scan size of 10 × 10 μm^2. All measurements have been performed in tapping mode (Nanoscope IIIa, (Veeco, Inc.). Classical silicon cantilevers were used (NCH, nanosensors). The average force constant and resonance were approximately 40 N/m and 300 kHz, respectively. The cantilever was excited at its resonance frequency. The AFM image processing was done using the Gwyddion V2.36 program which allows, among others, calculation of the roughness of the surface (RMS).

The scotch tape method [15] was used to estimate the adhesion of the structures to the substrate. This test is highly qualitative but it allows screening films involving poor adhesion from those where adhesion is appreciable. We pressed the tape onto the film and then rapidly stripped it. Three possibilities arise: (a) the film is completely removed from the substrate (b) the film is not at all removed, and (c) the film is partly removed or removed in patches. In the present work, the results of the scotch tape tests are evaluated through this classification. WO_3 films were examined using XPS technique. The quantitative study of WO_3 films was based on the determination of the $W4f_{7/2}$ and O1s peak areas with 1.26 and 0.61 as relative sensitivity factors (RSF) respectively.

The flexibility of the W/A/W structures was analyzed by a laboratory made bending test system. The samples were clamped between two parallel plates. One plate was mounted to the shaft of the motor, the other was fixed to a fixed support. The distance between the plates in the stretched mode was 25 mm. The bending radius was around 6 mm and the bending frequency was 1 Hz. During the bending test, the resistance of the samples was measured by an ohmmeter.

2.2. Realization and characterization of devices using W/A/W multilayer electrodes

To test the potential of the W/A/W multilayer structures as electrodes in the OPVCs we have made OPVCs using the planar heterojunction geometry. To this end, we used a structure that we have probed in the past, namely [28]:

Glass substrate/transparent anode/MO_3/CuI/ED/C_{60}/Alq_3/Al.

In these structures, the couple MO_3/CuI is the hybrid hole transporting layer (HTL), MO_3 corresponding to MoO_3 or WO_3. Alq_3 is the exciton blocking layer (EBL), Al the cathode, while ED is the electron donor and C_{60} is the electron acceptor of the junction of the OPVC. We took advantage of the present study to test a new ED, the dye based on A-π-D molecule, the (E)-2-cyano-3-(5-((E)-2-(9,9-diethyl-7-(methyl(phenyl)amino)-9H-fluoren-2-yl) vinyl)thiophen-2-yl)acrylic acid (M8-1). The synthesis of this new molecule M8-1 was already described [29]. It was recently synthesized with the aim of using it as an organic dye in solar cells. It was already shown that it is the most promising of a new family of dipolar A-π-D molecules [29]. With regard to the anode, we used our W/A/W multilayer structures, and also ITO anode as reference OPVCs. The ITO thin film was 100 nm thick and its sheet resistance was 20 Ω/sq.

The electrical characterization of the OPVCs was performed with an I-V tester, in the dark and under sun global AM 1.5 simulated solar illumination.

The second device used to probe the performance of the W/A/W multilayer structures was the Transparent Heat Mirrors (THM). A THM consists in a thin coating on a glass substrate which can transmit in the visible range and reflects in the near-infrared (NIR) and infrared (IR) range. Therefore a good THM must exhibit a maximum transmission of the visible light and maximum reflection in NIR and IR regions. Such THM can be used in energy efficient windows [30,31]. It was already shown that multilayer structures using high reflecting metal layers sandwiched between two high refractive index oxides such as ITO/Ag/ITO enhance the spectral selectivity [32]. Therefore, the refractive index of WO_3 [33] being similar to that of ITO [34], we checked the transmission and reflexion of our W/A/W structure in the visible, NIR and IR regions, the thickness of Ag film being used as parameter.

The third device grown with our W/A/W multilayer structures was the Transparent Heaters (THs). THs are electrically conducting thin film materials that are used to convert electrical energy into thermal energy on a surface which is transparent to visible light [35]. THs are used there where visibility and heating are required simultaneously: window defroster, outdoor panel display. Usually, ITO is the transparent conductive electrode in such devices. W/A/W multilayer structures are one of the possible substituent to ITO in these devices. The electrodes of the devices, two parallel contacts on opposite sides, were designed following the optimum disposition described elsewhere [35]. Two aluminium electrodes, spaced 1 cm apart, were deposited via a thermal evaporator system. The electrode thickness was 100 nm. The temperature measurements were taken via copper/constantan thermocouples.

3. Results and discussion

3.1. W/A/W multilayer characterization

Fig. 1 shows the optical transmission spectra with increasing Ag thickness. The variation of the transmission with the silver film thickness is classical for this kind of D/M/D structures, the transmission increases with the silver thickness up to an optimum value and then it decreases. The optimum thickness corresponds to the formation of a continuous Ag film. Below this thickness there is some absorption due to aggregated Ag islands. When the silver layers are less than 8 nm thick, they consist in grains which induces light scattering (See supporting information S 1-a). Then, 8–14 nm thick Ag films shows connected channel shape (See supporting information S 1-b), the light scattering effect of the grains decreases, until the film becomes completely continuous [36].

In the present experimental conditions the silver films become continuous for a thickness of 16 nm. The maximum transmission is 91.5% while its averaged value between 400 nm and 700 nm is 80.6%. A further increase of the silver thickness induces a decrease of the transmission. Nevertheless, in this thickness range of the silver layer the average transmission from 400 nm to 700 nm varies only slightly since it is 79.5% and 79.6% in the case of 14 nm and 18 nm respectively. As far as the maximum value of the transmission, it is 84.5% and 88.2% for 14 nm and 18 nm respectively. For more distant values, 12 nm and 20 nm the maximum transmission are 78.5% and 81.2% the averaged transmissions 71.05% and 72.46% respectively. In the inset of Fig. 1 we can see the variation of the sheet resistance of the W/A/W structures when the Ag film thickness increases from 12 nm to 20 nm. Here also a classical behaviour is obtained. The sheet resistance, R_s, decreases when the silver film thickness increases, first, quickly up to the percolation of the silver film, *i.e.* for 16 nm ($R_s = 8\,\Omega$/sq), then it stabilizes or decreases very slowly. The fact that the four point technique used to measure the sheet resistance allows measuring the whole structure and not only to the top dielectric layer was already addressed which is recalled in the supporting information S2. Therefore, the optimum Ag thickness in the W/A/W structures is 16 nm. The maximum value of the figure of merits (Φ_{TC}) suggested by Haacke [37] was calculated, Φ_{TC} being defined as:

$$\Phi_{TC} = T^{10}/R_s \quad (1)$$

with T transmission and R_s the sheet resistance of the W/A/W multilayer structure. The maximum obtained value is $\Phi_{TC} = 51\ 10^{-3}\,\Omega^{-1}$ and, using the T averaged transmission value between 400 nm and 700 nm, $\Phi_{TC} = 27\ 10^{-3}\,\Omega^{-1}$, values which are situated in the expected range for this kind of structures [21]. For 14 nm and 18 nm the averaged values are $3\ 10^{-3}\,\Omega^{-1}$ and $14\ 10^{-3}\,\Omega^{-1}$ respectively, while for 12 nm and 20 nm they are $1.6\ 10^{-4}\,\Omega^{-1}$ and $11\ 10^{-3}\,\Omega^{-1}$. The quite small Φ_{TC} value obtained with 12 nm of Ag is due to the fact that this thickness is situated just before the percolation of the silver film and Rs is still 200 Ω/sq, while it is 7 Ω/sq for 20 nm of silver.

In Fig. 2, the XRD pattern of Glass/W/A/W structure, with 16 nm of Ag, has a peak at $2\theta = 38.1°$ that corresponds to (111) plane of Ag (JCPDS N° 87-0720). No peaks due to WO_3 are visible which means that WO_3 layers are amorphous.

The surface visualization by SEM of the Glass/W/A/W multilayer structures is shown in Fig. 3. The structure appears smooth and quite

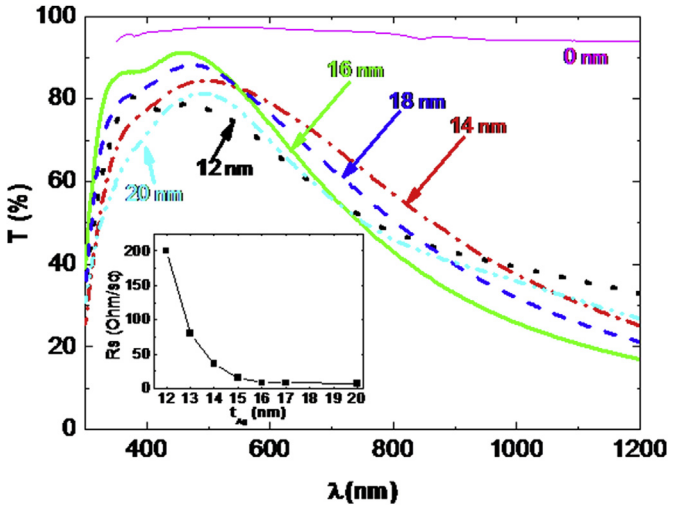

Fig. 1. Variation of the transmission of Glass/W (20 nm)/A (x nm)/W (35 nm) structures with the thickness of the Ag layer.
Inset Figure 1: Variation of the sheet resistance of these structures.

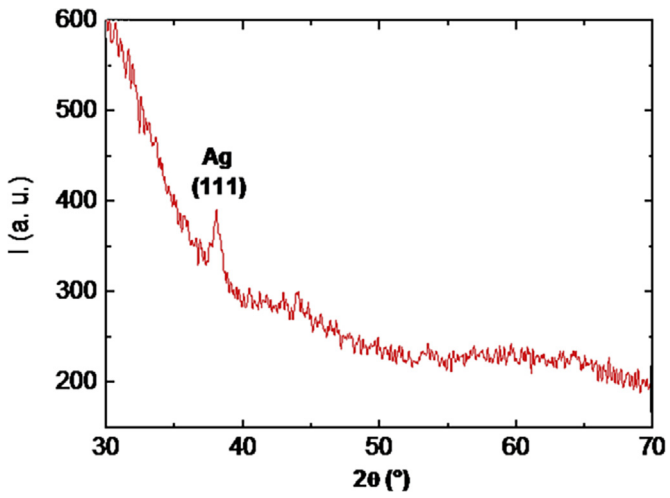

Fig. 2. X-Ray diffraction diagram of Glass/W (20 nm)/A (16 nm)/W (35 nm).

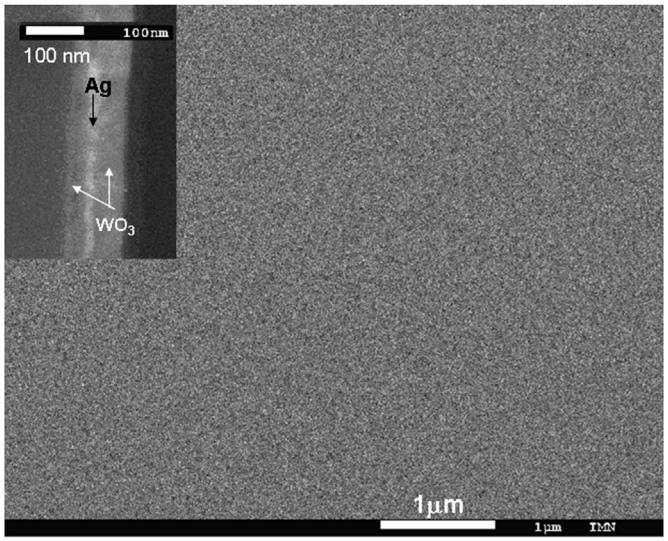

Fig. 3. Visualization of the surface of a Glass/W (20 nm)/A (16 nm)/W (35 nm) structure.
Insets: Left side, cross section of this structure.

homogeneous without defects such as pinholes, cracks or pinholes owing to the stable amorphous structure and the very fine particle shape of the WO_3 top layer. The cross section visualized in the left insert, shows that the three layers of the structure are clearly visible. Moreover, that cross section shows clearly the continuity of the metal interlayer. It must be noted that the structures are slightly blue coloured due to the oxygen deficiency of the WO_3 layers [38]. As a matter of fact, the XPS study shows that there is some oxygen deficiency in WO_3 layers, such deficiency is usual in transition metal films deposited by sublimation under vacuum [39].

Fig. 4 shows the XPS peaks corresponding to O1s (Fig. 4a) and W4f (Fig. 4b) of a WO_3 layer deposited by sublimation process on a glass substrate. Fig. 4a shows that O1s peak is asymmetric which means that it corresponds to several contributions. It can be de-convoluted into two peaks situated at 530.8 eV and 531.9 eV. Knowing that the reference carbon peak, C1s, is located at 284.8 eV, the lower binding energy at 530.8 eV is attributed to oxygen bounded to W, corresponding to fully oxidized WO_3. The higher energy of O1s peak appearing at 531.9 eV can be assigned to oxygen vacancies and hydroxyl group due to surface contamination. However, different authors have already associated the high energy O1s peak, situated around 531.9 eV, to oxygen deficient regions in oxides [40,41]. The contribution of oxygen vacancies to the O1s high energy peak is corroborated by W3d peak deconvolution. The Fig. 4b shows that two doublets are necessary to obtain a good agreement between the experimental and theoretical curves. The two mains peaks visible in Fig. 4b, situated at 36.1 and 38.2 eV, can be attributed to $W4f_{7/2}$ and $W4f_{5/2}$ of WO_3. The binding energy difference between the two peaks of the doublet, 2.1 eV is in accordance with the standard reference value [42]. In addition to this contribution due to the W in the W^{6+} oxidation state, a second doublet of lower intensity assigned at 35 and 37.1 eV can be attributed to W^{5+} ion, contribution which corresponds to oxygen vacancies.

The survey scan (Supporting information S3) of the top layer of a W/A/W multilayer structure consists of peaks corresponding to W, O and surface C. The curve shows that there is no Ag metal on the top. The homogenous dielectric layer is retained over the continuous mid metal layer of the W/A/W multilayer structure.

The homogeneity of the W/A/W multilayer structures was checked by AFM study. The surface topography of a Glass/W/A/W multilayer structure was measured by AFM and using $3 \times 3\ \mu m^2$ scans (Supporting information S4). The root mean square surface roughness (rms) is 1.72 nm. Such small rms confirms the impression of high homogeneity

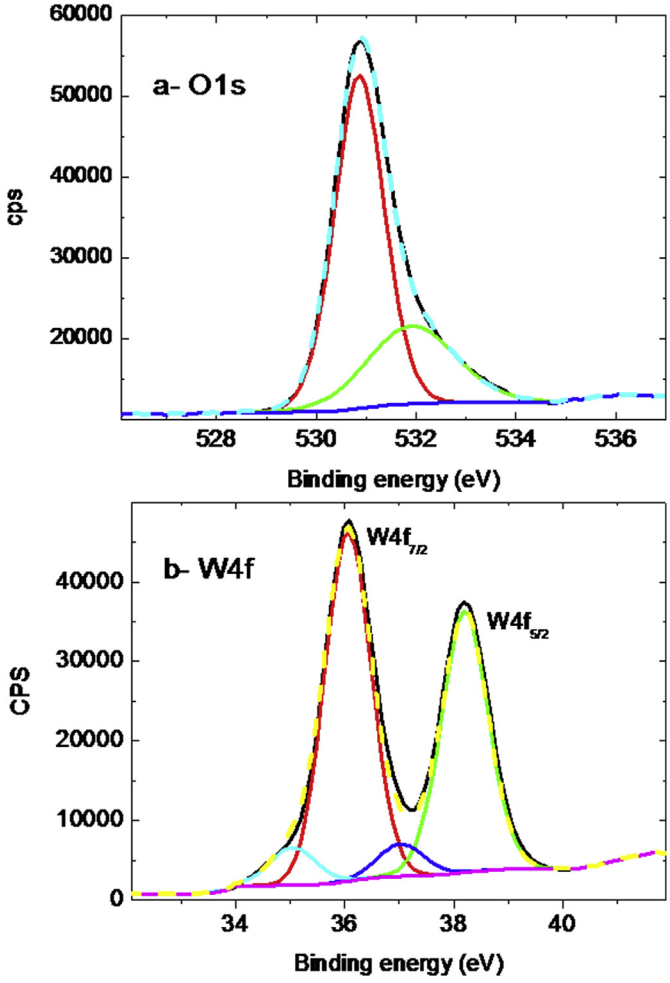

Fig. 4. XPS spectra of O1s (a) and W4f (b) of the surface of a WO_3 layer.
Dotted curves: Measured curves.
Continuous lines: Theoretical curves.

resulting from the visualization by SEM.

The structures deposited onto glass substrates pass the scotch tape test. Actually, the multi-layer structures are systematically not removed at all.

About the flexibility, our bending apparatus is able to perform outer and inner bending tests. For inner bending, the sample was loaded with the multilayer structure facing downward, while for outer bending measurements, the sample was loaded with the multilayer structure facing upward.

In order to check and evaluate the flexibility of our W/A/W structures onto PET substrates, we tested them under outer and inner bending as described above. The results are compared to commercial 100 nm-thick ITO onto PET thick of 125 µm.

During the bending tests, the variation of the sheet resistance of the PET/W/A/W and PET/ITO samples was measured after 1, 5, 15, 25, 50, 100, 500, 1000 and 2000 cycles. The change in resistance was expressed as $(R\text{-}R_0)/R_0$, where R_0 is the initial resistance and R the measured resistance after bending. Whatever the sample, PET/ITO or PET/W/A/W, it has nearly the same behaviour when it is submitted to inner or outer bending (Supporting information S5). The sheet resistance of PET/ITO increases continuously with the number of cycles, while it is nearly stable in the case of PET/W/A/W. More precisely, for outer bending, in the case of W/A/W multilayer structures there is not any variation of the sheet resistance after 2000 cycles, except some few samples which exhibit an increase of 1% or less. For comparison, the $(R\text{-}R_0)/R_0$ value of the PET/ITO sample increases regularly from the first

cycle. For instance, the value of $(R-R_0)/R_0$ in the case of outer bending is 25% after 50 cycles and 160% after 500 cycles (Supporting information S5). It must be noted that, in the case of ITO, the thickness of the PET substrate was 125 μm, which is of the same order of magnitude than that used for the W/A/W multilayer structures (150 μm). We can therefore compare the results obtained, especially since the finer the substrate and the lower the stress. As a matter of fact, it is known that the minimum allowed radius of curvature scales linearly with the total thickness of the sample [43].

The good stability of the sheet resistance of the PET/W/A/W multilayer structures can be attributed to the presence of the ductile Ag metal layer between the WO_3 layers and to the fact that WO_3 being amorphous, unlike ITO (see supporting information S6), its failure strain is higher than that of crystalline films.

Moreover, it must be noted that W/A/W multilayer structures deposited onto PET also pass the scotch test. Herein, the multilayer structures are systematically not removed at all, which testifies that, even on PET substrates, W/A/W multilayer structures present an excellent adhesion.

The properties of W/A/W multilayer structures, listed above, make it possible to envisage using them in various devices and we give some examples below.

3.2. Use of the W/A/W multilayer electrode in various applications

In a first attempt, a W/A/W multilayer structure was substituted to ITO as transparent conductive anode in organic photovoltaic cells (OPVCs). As said above, an OPVC device is a sandwiched structure containing two electrode layers and an organic active layer in the middle. The active layer consists of one electron donor material and one electron acceptor either in the form of stacked layers or bulk heterojunctions. Here, for simplicity, we used stacked layers deposited under vacuum. Often, in classical structures the top cathode is an aluminum layer, which behaves like a mirror for unabsorbed light and the bottom anode is the transparent conductive electrode. In the present work, the anode was a W (20 nm)/A (16 nm)/W (15 nm) multilayer structure or, as reference, ITO. As specified in paragraph 2.2, the OPVCs were completed using the HTL MoO_3/CuI and the EBL Alq_3, while the active organic couple was M8-1/C_{60}. Therefore the OPVCs probed were as follows:

Substrate/transparent anode Glass/(W/A/W or ITO)/MoO_3/CuI/M8-1/C_{60}/Alq_3/Al.

The results obtained are presented in Table 1 and Fig. 5.

It is a first series of results obtained with the new molecule M8-1 and it remains to optimize its performance by working on its deposition parameters (deposition rate, thickness of the layer …) it nevertheless remains that the results are significant for the effectiveness of the W/A/W multilayer structure as TCE. Not only is the efficiency of the OPVCs practically the same, whatever the TCE, ITO or W/A/W structure, but the shape of the curves is remarkably similar, which shows that the ITO can be substituted by the W/A/W without degradation of OPVCs performance. It must be noted that the presence of the MO_3/CuI hole transporting layer allows achieving high hole collection efficiency.

In a second attempt, W/A/W multilayer structures were probed as THM. A change of 2 nm in the Ag layer thickness modifies significantly the transmission and the reflection of the structures. Ag is highly reflecting in NIR and IR regions, while its transmission in the visible depends strongly on its thickness. Ag layer must be thick enough to

Table 1
Parameters of the OPVCs.

Anode	Voc (V)	J (mA/cm^2)	FF (%)	η (%)
ITO	0.69	2.54	38	0.67
W/A/W	0.67	2.44	39	0.62

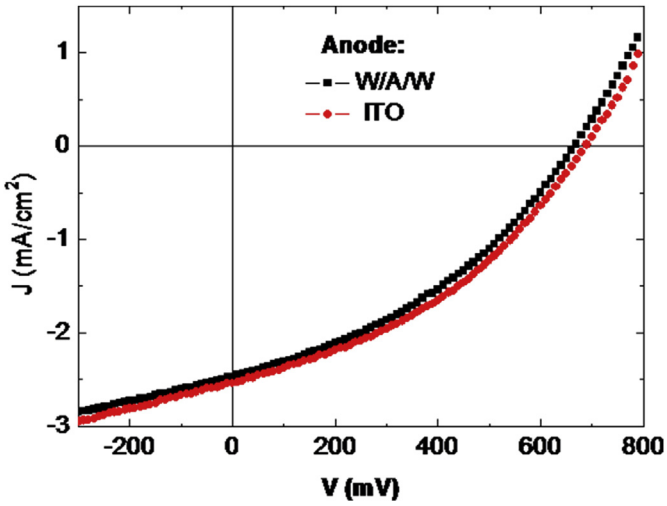

Fig. 5. J-V characteristics of an OPVC with Glass/ITO (●) and Glass/W/A/W (■) as anode.

achieve good reflection in NIR and IR regions, but it must be thin enough to allow high transmission in the visible domain. Therefore, there is an optimum compromise between the transmission and the reflection to achieve the highest possible efficiency as THM. It is known that, when W/A/W multilayer structures are used as THM, the Ag layer must be continuous to exhibit a good selectivity and stability [44]. In the present work, we saw that the Ag film becomes continuous for a thickness of 16 nm. Therefore we probe structures with Ag layer thickness equal to 16 nm and more, while those of WO_3 layers were 20 nm and 35 nm for the bottom and top layer respectively. The Fig. 6 shows that, when the Ag thickness is 16 nm, the transmission in the visible is very high but the reflection in the NIR and IR is quite weak. For Ag thickness of 20 nm, the reflection is good, but the transmission is significantly lowered. Therefore, the optimum Ag thickness in the W/A/W multilayer structures, when they are used as THM, is 18 nm.

In a third attempt, W (20 nm)/A/W (35 nm) multilayer structures were probed as transparent heater, the thickness of Ag layer being, here also, used as parameter. Samples with different sheet resistance, 8, 36, 85 and 200 Ω/sq were probed in order to study the influence of the sheet resistance on the structure performance. These sheet resistances correspond to Ag layer thickness of 16 nm, 14 nm, 13 nm and 12 nm respectively.

In Fig. 7a, the change in steady state temperature of the THs with respect the applied voltage is shown, it can be seen that dependence of the temperature with the applied voltage depends strongly of the sheet

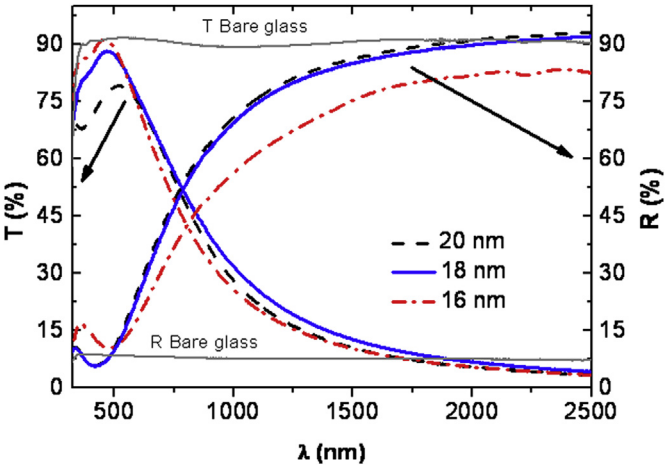

Fig. 6. Transmission and reflectivity of Glass/W/A/W multilayer structures.

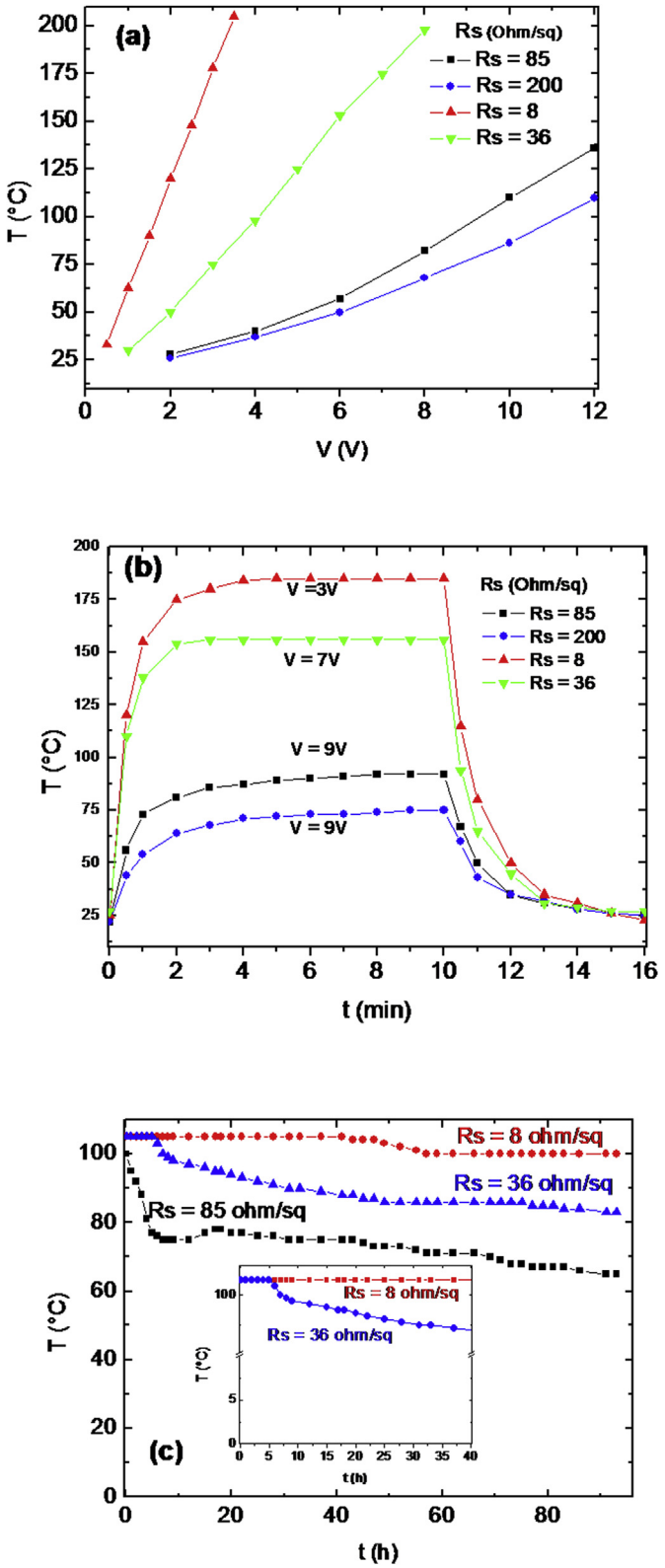

Fig. 7. (a) Variation of the steady state temperature with the applied voltage, the sheet resistance of the structures being used as parameter, (b) Temperature variation with time at a constant applied voltage, the sheet resistance of the structures being used as parameter, (c) Variation of the temperature as a function of time. Inset: Variation during the first 40 h of operation.

resistance of the structure, while only 3.5 V are needed to reach 205 °C for a sample with 8 Ω/sq as sheet resistance, 12 V are necessary to achieve 110 °C for a sample with 200 Ω/sq as sheet resistance. Actually, the variation of the steady state temperature with the applied voltage is controlled by the Joule's law:

$$P = V^2/R \quad (2)$$

With P the power, V the applied voltage and R the resistance.

Therefore, samples with smaller sheet resistance can reach higher temperature under the same applied bias. This is consistent with the fact that higher heat dissipation can be obtained for sample with smaller sheet resistance under a fixed bias (Fig. 7b).

Fig. 7b shows the time-dependent thermal response of the different W/A/W multilayer structures for a constant applied voltage of 9 V for samples with the higher sheet resistance values (200, 85 Ω/sq), 7 V for the sample which sheet resistance is 36 Ω/sq and 3 V for 8 Ω/sq. It can be seen in Fig. 7b, that the heating and cooling time constant are similar whatever the sheet resistance of the sample is, but the maximum temperature reaches is quite different, which makes that the heating and cooling rates are significantly different. During the first minute, the heating rate is 2.2 °C per second for the most conductive sample, and only 0.5 °C for the sample with the highest sheet resistance. Similarly the cooling rate is −1.2 °C and – 0.85 °C in the former and latter case respectively.

Finally, we have studied the stability of these structures; the results are synthesized in Fig. 7c. Here also, the voltage chosen to follow the ageing of the devices depends of the sheet resistance of the structure. It can be seen that the stability of the structures depends significantly on the sheet resistance of the structures. Here also the best performance is obtained with the sample with the smaller sheet resistance.

The performance, as transparent heater, of the W/A/W structure can be compared with those obtained with another possible ITO substituent, the silver nanowires thin films (AgNWs) [35]. The performance of the AgNWs layers depend significantly on the AgNWs density, *i.e.* with the sheet resistance of the films. The steady state temperatures achieved with the applied voltage by the AgNWs films are similar to those achieved in the present work for equivalent sheet resistance. Similarly, the heating and cooling rates of the samples are similar. About the ageing process, the stability of the W/A/W structure with the smaller sheet resistance (8 Ω/sq) is similar to that of the AgNWs films (see inset Fig. 7c). Moreover, we proceeded to longer experiment and we showed that after one week of continuous operation, the loss in temperature is only 5%, which testifies of the stability of W/A/W multilayer structures. Such high life time, compared to that of AgNWs single layer, can be attributed to the protective effect of the WO_3 layers which surround the Ag layer in our structures W/A/W. Actually, it was shown recently that, in the case of OPVCs, the lifetime of the devices with WO_3/Ag or W/A/W devices as top electrodes was quite different. When WO_3/Ag is used as top electrode there is de-wetting of the electrode, while there is not in the case of W/A/W top electrode [45]. Therefore it is necessary to use sample with very small sheet resistance to obtain performing transparent heater. Moreover, it is necessary to insert the conductive layer between protective oxide layers to improve the device lifetime.

4. Conclusion

Simple deposition by Joule effect of W/A/W multilayer structures, allows achieving performing structures which can be introduced in different devices. The optimum averaged figure of merit of the W (20 nm)/A (16 nm)/W (35 nm) structure is $\Phi_{TC} = 27\ 10^{-3}\ \Omega^{-1}$. We have probed these structures in different devices. The OPVCs using the W (20 nm)/A (16 nm)/W (35 nm) multilayer structure as transparent anode, achieve efficiency similar to that reach with ITO anodes. For a slightly thicker Ag film, the W (20 nm)/A (18 nm)/W (35 nm) multilayer structures reach optimal transmission and reflection for use as

THM. The use of these structures as stable TH implies that their sheet resistance is as small as possible in order to obtain performance similar to those reach by AgNWs layers. It is the case of W (20 nm)/A (16 nm)/W (15 nm) multilayer structures which sheet resistance is 8 Ω/sq. It can be concluded that these W/A/W structures are very easy to use, since it suffices to optimize the thickness of Ag as a function of the required structure and to adapt the upper oxide layer to the desired application. For instance, in the case of OPVCs, the optimum top WO_3 layer thickness is 15 nm (Supporting information S2). When covered by MO_3/CuI hole transporting layer it behaves as efficient anode due to the high work function of this hybrid buffer layer. If it was covered with a layer of material of which work function is weak, such as Ca, CsI, Cs_2CO_3, it could then be used as a cathode collecting electrons. When used as TH, the presence of the WO_3 layers between which that of Ag is inserted, makes it possible to obtain a longer lifetime than that of structures using simple silver layer.

Acknowledgements

The authors acknowledge funding from the European Community ERANETMED_ENERG-11-196: Project NInFFE, ECOS-CONICYT action n° C14E05 and from CNRST (PPR/2015/9) Ministère, Morocco).

Appendix A. Supplementary data

Supplementary data related to this article can be found at http://dx.doi.org/10.1016/j.vacuum.2018.04.026.

References

[1] C.G. Granqvist, Transparent conductors as solar energy materials: a panoramic review, Sol. Energy Mater. Sol. Cells 91 (2007) 1529–1598.
[2] H. Liu, V. Avrutin, N. Izyumskaya, Ü. Özgür, H. Morkoç, Transparent conducting oxides for electrode applications in light emitting and absorbing devices, Superlattice. Microst. 48 (2010) 458–484.
[3] H. Hosono, Recent progress in transparent oxide semiconductors: materials and devices application, Thin Solid Films 515 (2007) 6000–6014.
[4] G.J. Exarhos, X.-D. Zhou, Discovery-based design of transparent conducting oxide films, Thin Solid Films 515 (2007) 7025–7052.
[5] S.D. Senol, A. Senol, O. Ozturk, M. Erdem, Effect of annealing time on the structural, optical and electrical characteristics of DC sputtered ITO films, J. Mater. Sci. Mater. Electron. 25 (2014) 4992–4999.
[6] J. Gwamuri, A. Vora, J. Mayandi, D.Ö. Guney, P.L. Bergstrom, J.M. Pearce, A new method of preparing highly conductive ultra thin indium tin oxide for plasmonic-enhanced thin film solar photovoltaic devices, Sol. Energy Mater. Sol. Cells 149 (2016) 250–257.
[7] L. Baia, M. Quintela, L. Mendes, P. Nunes, R. Martins, Performance exhibited by large area ITO layers produced by r.f, Magnetron Sputtering Thin Solid Films 337 (1999) 171–175.
[8] Ü. Özgür, Ya I. Alivov, C. Liu, A. Teke, M.A. Reshchikov, S. Doğan, V. Avrutin, S.-J. Cho, H. Morkoç, Applied physics reviews, A comprehensive review of ZnO materials and devices, J. Appl. Phys. 98 (2005) 041301.
[9] A. Klein, C. Körber, A. Wachau, F. Säubeerlich, Y. Gassenbauer, S.P. Harvey, D.E. Proffit, T.O. Mason, Transparent conducting oxides for photovoltaics: manipulation of Fermi level, work function and energy band alignment, Materials 3 (2010) 4892–4914.
[10] H.-K. Park, J.-W. Kang, S.-I. Na, D.-Y. Kim, H.-K. Kim, Characteristics of indium-free GZO/Ag/GZO and AZO/Ag/AZO multilayer electrode grown by dual target DC sputtering at room temperature for low-cost organic photovoltaics, Sol. Energy Mater. Sol. Cells 93 (2009) 1994.
[11] C. Guillén, J. Herrero, TCO/metal/TCO structures for energy and flexible electronics, Thin Solid Films 520 (2011) 1–17.
[12] L. Cattin, J.C. Bernède, M. Morsli, Toward indium-free optoelectronic devices: dielectric/Metal/Dielectric alternative conductive transparent electrode in organic photovoltaic cells, Phys. Status Solidi A 210 (2013) 1047–1061.
[13] G. Leftheriotis, S. Papaefthimiou, P. Yianoulis, Integrated low-emittance-electrochromic devices incorporating ZnS/Ag/ZnS coatings as transparent conductors, Sol. Energy Mater. Sol. Cells 61 (2000) 107–112.
[14] W. Greenbank, L. Hirsch, G. Wantz, S. Chambon, Interfacial thermal degradation in inverted organic solar cells, Appl. Phys. Lett. 107 (2015) 263301.
[15] M. Hssein, S. Tuo, S. Benayoun, L. Cattin, M. Morsli, Y. Mouchaal, M. Addou, A. Khelil, J.C. Bernède, Cu-Ag bi-layer films in dielectric/metal/dielectric transparent electrodes as ITO free electrode in organic photovoltaic devices, Org. Electron. 42 (2017) 173–180.
[16] M. Hssein, L. Cattin, M. Morsli, M. Addou, J. C. Bernède, Importance of the electrode conductivity in organic photovoltaic solar cells, J. Mater. Sci. Mater. Electron. https://doi.org/10.1007/s10854-016-5973-4.
[17] C. Tao, G. Xie, C. Liu, X. Zhang, W. Dong, F. Meng, X. Kong, L. Shen, S. Ruan, W. Chen, Semitransparent inverted polymer solar cells with MoO3/Ag/MoO3 as transparent electrode, Appl. Phys. Lett. 95 (2009) 053303.
[18] W.-F. Xu, C.-C. Chin, D.-W. Hung, R.-K. Wei, Transparent electrode for organic solar cells using multilayer structures with nanoporous silver film, Sol. Energy Mater. Sol. Cells 118 (2013) 81–89.
[19] N.P. Sergeant, A. Hadipour, B. Niesen, D. Cheyns, P. Heremans, P. Peumans, B.P. Rend, Design of transparent anodes for resonant cavity enhanced light harvesting in organic solar cells, Adv. Mater. 24 (2012) 728–732.
[20] K. Hong, K. Kim, S. Kim, I. Lee, H. Cho, S. Yoo, H.-W. Choi, N.-Y. Lee, Y.-H. Tak, J.-L. Lee, Optical properties of WO_3/Ag/WO_3 multilayer as transparent cathode in top-emitting organic light emitting diodes, J. Phys. Chem. C 115 (2011) 3453–3459.
[21] B. Lin, C. Lan, C. Li, Z. Chen, Effect of thermal annealing on the performance on WO_3/Ag/WO_3 transparent conductive film, Thin Solid Films 571 (2014) 134–138.
[22] E. Koubli, S. Tsakanikas, G. Leftheriotis, G. Syrrokostas, P. Yianoulis, Optical properties and stability of near-optimum WO_3/Ag/WO_3 multilayers for electrochromic applications, Solid State Ionics 272 (2015) 30–38.
[23] H. Li, Y. Lv, X. Zhang, X. Wang, X. Liu, High-performance ITO-free electrochromic films based on bi-functional stacked WO_3/Ag/WO_3 structures, Sol. Energy Mater. Sol. Cells 136 (2015) 86–91.
[24] Y. Yin, C. Lan, H. Guo, C. Li, Reactive sputter deposition of WO3/Ag/WO3 film for Indium Tin Oxide (ITO)-free electrochromic devices, ACS Appl. Mater 8 (2016) 3861–3867.
[25] E. amendola, A. Cammarano, M. Pezzuto, D. Acierno, Adhesion of functional layer on polymeric substrates for optoelectronic applications, J. Eur. Opt. Soc. 4 (2009) 09027.
[26] D.-T. Nguyen, S. Vedraine, L. Cattin, P. Torchio, M. Morsli, F. Flory, J.C. Bernède, Effect of the thickness of the MoO3 layers on optical properties of MoO3/Ag/MoO3 multilayer structures, J. Appl. Phys. 112 (2012) 063505.
[27] L. Cattin, Y. Lare, M. Makha, M. Fleury, F. Chandezon, T. Abachi, M. Morsli, K. Napo, M. Addou, J.C. Bernède, Effect of the Ag deposition rate on the properties of conductive transparent MoO_3/Ag/MoO_3 multilayers, Sol. Energy Mater. Sol. Cells 117 (2013) 103–109.
[28] Y. Berredjem, N. Karst, L. Cattin, A. Lkhdar-Toumi, A. Godoy, G. Soto, F. Diaz, M.A. del Valle, M. Morsli, A. Drici, A. Boulmokh, A.H. Gheid, A. Khelil, J.C. Bernède, Plastic photovoltaic cells encapsulation, effect on the open circuit voltage, Dyes Pigments 78 (2008) 148–156.
[29] E. Ortega, R. Montecinos, L. Cattin, F.R. Díaz, M.A. del Valle, J.C. Bernède, Synthesis, characterization and photophysical-theoretical analysis of compounds A-π-D. 1. Effect of alkyl-phenyl substituted amines in photophysical properties, J. Mol. Struct. 1141 (2017) 615–623.
[30] G. Leftheriotis, P. Yianoulis, D. Patrikios, Deposition and optical properties of optimised ZnS/Ag/ZnS thin films for energy saving applications, Thin Solid Films 306 (1997) 92–99.
[31] C.G. Granquist, Radiative heating and cooling with spectrally selective surface, Appl. Optic. 20 (1981) 2606–2615.
[32] K.P. Sibin, N. Selakumar, A. Kumar, Arjun Dey, N. Sridhara, H.D. Shashikala, A.K. Sharma, H.C. Barshilia, Design and development of ITO/Ag/ITO spectral beam splitter coating for photovoltaic-thermoelectric hybrid systems, Sol. Energy 141 (2017) 118–126.
[33] M.C. Rao, O.M. Hussain, Optical properties of vacuum evaporated WO_3 thin films, Res. J. Chem. Sci. 1 (2011) 76–80.
[34] X. Yan, F.W. Mont, D.J. Poxson, M.F. Schubert, J.K. Kim, J. Cho, E.F. Schubert, Refractive-index-matched indium–tin-oxide electrodes for liquid crystal displays, Jpn. J. Appl. Phys. 48 (2009) 120203.
[35] O. Ergun, S. Coskun, Y. Yusufoglu, H.E. Unalan, High-performance, bare silver nanowire network transparent heaters, Nanotechnology 27 (2016) 445708.
[36] J.-A. Jeong, H.-K. Kim, Al2O3/Ag/Al2O3 multilayer thin film aestivation prepared by plasma damage-free linear target sputtering for organic light emitting diodes, Thin Solid Films 547 (2013) 63–67.
[37] G. Haacke, New figure of merit for transparent conductors, J. Appl. Phys. 47 (1976) 4086–4089.
[38] G. Leftheriotis, G. Leftheriotis, P. Yianoulis, Study od electrochromic cells incorporating WO3, MoO3, WO3-MoO3 and V2O5 coatings, Thin Solid Films 343-344 (1999) 183–186.
[39] L. Fang, S.J. Baik, J.W. Kim, S.J. Kang, J.W. Seo, J.-W. Jeon, Y.H. Kim, K.S. Lim, Tunable work function of a WO_x buffer layer for enhanced photocattier collection of pin-type amorphous silicon solar cells, J. Appl. Phys. 109 (2011) 104501.
[40] J.C.C. Fan, J.B. Goodenough, X-ray photoemission spectroscopy studies of Sn-doped indium-oxide films, J. Appl. Phys. 48 (1977) 3524–3531.
[41] S.W. Heo, Y.D. Ko, Y.S. Kim, D.K. Moon, Enhanced performance in polymer light emitting diodes using an indium–zinc–tin oxide transparent anode by the controlling of oxygen partial pressure at room temperature, J. Mater. Chem. C 1 (2013) 7009.
[42] W. Grunert, E.S. Spiro, R. Feldhaus, K. Anders, G.V. Antoshin, K.M. Minachev, Reduction behavior and metathesis activity of WO_3/Al_2O_3 catalysts: I. An XPS investigation of $WO_3Al_2O_3$ catalysts, J. Catal. 107 (1987) 522.
[43] Z. Suo, E.Y. Ma, H. Gleskova, S. Wagner, Mechanics of rollable and foldable film-on-foil electronics, Appl. Phys. Lett. 74 (1999) 1177–1178.
[44] Z. Wang, X. Cai, Q. Chen, L. Li, Optical properties of metal dielectric multilayers in the near uv region, Vacuum 80 (2006) 438–443.
[45] W. Greenbank, L. Hirsch, S. Chambon, Electrode de-wetting as a failure mechanism in thermally-aged OPV devices, Sol. Energy Mater. Sol. Cell. 178 (2018) 8–14.